

Research Article

Influence of Muscle Contraction on Pedestrian Injury in Pickup-Truck Collision

Putu Alit Putra

Automotive Safety and Assessment Research Centre, The Sirindhorn International Thai-German Graduate School of Engineering, King Mongkut University of Technology North Bangkok Thailand
Institute of General Mechanics (IAM), RWTH Aachen University, Germany

Bernd Markert

Institute of General Mechanics (IAM), RWTH Aachen University, Germany

Julaluk Carmai*

Automotive Safety and Assessment Research Centre, The Sirindhorn International Thai-German Graduate School of Engineering, King Mongkut University of Technology North Bangkok Thailand

* Corresponding author. E-mail: julaluk.c@tggs.kmutnb.ac.th

DOI: 10.14416/j.asep.2025.12.001

Received: 21 July 2025; Revised: 25 August 2025; Accepted: 8 October 2025; Published online: 1 December 2025

© 2025 King Mongkut's University of Technology North Bangkok. All Rights Reserved.

Abstract

Pedestrian safety remains a major public health concern. Although numerical human body models are widely used in the automotive industry, most lack active muscle representation, a factor that can influence body kinematics during low-speed collisions. This study investigates how skeletal muscle activation impacts pedestrian kinematics and injury. A skeletal muscle model combining 3D tetrahedral and 1D line elements was developed. Passive behavior was modeled using the Ogden model, while active behavior was based on the Hill-type muscle model. The model was validated against published data and integrated into a finite element pedestrian model. Four levels of muscle activation were applied to examine their effects on kinematics and injury metrics. Active muscle significantly influences pedestrian response during collisions. Models with active muscle demonstrated higher contact forces, head injury criteria, lower extremity bending moments, and knee shear distance but lower knee bending angles. For instance, at 20 km/h, comparing passive to fully active models revealed a significant 179% increase in Head Injury Criterion (HIC), a 10% decrease in knee bending angle, and a 7.7% increase in shear distance. Varying activation levels had a minimal effect on lower extremity forces and moments but influenced HIC and knee metrics. The same trends were observed at higher impact speeds. These results underscore that including active muscle behavior is essential for accurate pedestrian injury prediction in low-speed collisions.

Keywords: Active muscle, Finite element simulation, Human body model, Pedestrian, Vehicle safety

1 Introduction

Globally, collisions between vehicles and pedestrians are a significant challenge for public health and road safety, accounting for 22% of all traffic collisions [1]. Urban areas, where vehicle-pedestrian interactions are frequent, are particularly high-risk zones. While many efforts have been made to mitigate pedestrian injuries, most improvements in vehicle design, such as more pedestrian-friendly front bumpers and bonnets, have

focused on passenger cars. However, pickup trucks, which made up 17% of vehicle registrations in Thailand in 2021 [2], are also commonly used for passenger transport in urban areas where average speeds range from 17.6–21.8 km/h [3]. This increases the chance of pedestrian interactions. Since the kinematics and injury patterns of passenger car-pedestrian impacts differ from those of pickup truck-pedestrian impacts, developing effective modifications requires a thorough understanding of these dynamics.

To gain this understanding, crash experiments or, more commonly, numerical simulations are used. The use of virtual finite element human body models has gained increasing attention in the automotive industry. Many manufacturers now employ these models during the design stage to evaluate the performance of crashworthiness structures and safety systems. To date, several finite element human body models have been developed to simulate the roles of occupants and pedestrians in automotive safety [4]. Several researchers have already conducted studies on vehicle-pedestrian collisions using finite element human body models. However, most existing models were developed using cadaver data, which inherently lack active muscle function. Since cadaveric tissues cannot replicate reflexive contraction or neuromuscular activation, these models may underestimate real-world injury responses [4]–[6]. In a real-world panic situation, such as when a pedestrian sees an oncoming car, the body's natural fight response prepares for impact. This response leads to an increase in the contractions of fast-contracting skeletal muscles, which are stimulated either directly or through our motor nerves [7]. Including active muscle in the model allows for a more accurate approximation of a living pedestrian's response, as real humans reflexively contract their muscles in panic situations before an impact.

There have been attempts to develop active muscle models for separated body parts. Alvarez *et al.*, [8] and Hedenstierna *et al.*, [9] developed finite element model of neck muscles. They found that the muscle tonus affected the head impact location and direction. In addition, they reported that the Continuum muscle model was suitable for the impact simulations [8]. Iwamoto *et al.*, [10] studied a 3D active and passive muscle model in an occupant human body model. They found that the neck with active muscles could affect neck elongation, as well as head linear and angular acceleration. Soni *et al.*, [11] studied the effects of muscle contraction on the response of the lower extremity, focusing on lateral impacts and their effects on knee ligaments and bones. Various techniques have been proposed for active muscle modeling, including discrete Hill-type models [8], continuum muscle models [9], hybrid bar–solid element models [10], and 1D bar element approaches [11], [12]. However, most studies have focused on simplified geometries or isolated body regions, leaving a gap in tools that can evaluate whole-body pedestrian responses under realistic crash conditions. There is a clear need for human body models that

incorporate active muscle behavior to better predict kinematics and injury outcomes. To address this, the present study integrates 24 active skeletal muscles with 3D geometry into both legs of the Total Human Body Model for Safety (THUMS) pedestrian model, enabling whole-body simulations of low-speed impacts with varying activation levels. This approach provides a novel tool for the study of the influence of different levels of lower extremity muscle activation on pedestrian kinematics and injury in realistic crash scenarios. The 3D real geometry of the muscle was utilized in this study.

2 Materials and Methods

The model was developed in LS-Dyna through three main steps. First, active skeletal muscle models were created and validated for each lower extremity segment. Second, these muscles were then integrated into the THUMS, a model previously developed by Toyota Motor Corporation [13]. Finally, a vehicle-pedestrian collision model was established using the active muscle THUMS as the pedestrian.

2.1 Skeletal muscles model development and validation

The geometries of relevant skeletal muscles were obtained from the open-source BodyParts3D project [14], which is based on the size of an average Japanese male (172.8 cm in height and 65 kg in weight) [15]. These geometries were then modified to match the existing 50th-percentile THUMS model. In addition to geometry, the architectural properties of the muscles were needed. Muscle architecture, which refers to the physical arrangement of muscle fibers at a microscopic level, determines a muscle's functional capacity [16], [17]. These properties include the physiological cross-sectional area, which is the area of a muscle's cross-section perpendicular to its fibers. It's used to describe the contraction properties of pennate muscles [18]. The pennation angle, defined as the angle between fascicle orientation and the tendon axis, affects force transmission, with maximal contractile force produced at the optimal fiber length and pennation angle [19]. Peak isometric force is defined as the maximum force that can be produced by the muscle at its optimal length [19]. To accurately model the complex musculature of the lower extremities, we gathered comprehensive architectural properties, including muscle origins, insertions, and pennation angles from several publications [20]–[26]. These

references were essential for collecting the data required to build an accurate model. The active muscle models were developed by selecting geometries and meshing them for a 2D shell first and then converting the 2D shell into 3D solid tetrahedral elements. Shells served only as intermediate meshing surfaces for creating the muscle models' solid mesh. Once the 3D solid tetrahedral elements were generated, the 2D shell elements were deleted to avoid duplication and simplify the final model. The 1D beam element was created manually. The orientation of the 1D elements, which acted as muscle fibers, was set to be as similar as possible to the fiber orientation of real muscles.

Figure 1 illustrates an example of the muscle model with the fiber orientation. The muscle model was developed by a combination of 1D elements and 3D solid tetrahedral elements. Two-dimensional elements were not used because they cannot accurately represent the volumetric behavior or realistic fiber orientation that is critical for capturing muscle mechanics.

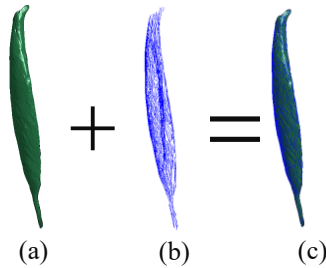


Figure 1: Active muscle model of Vastus lateralis (a) 3D solid element (b) 1D beam element (c) combination of 2D and 1D elements.

The Ogden material model was selected for the 3D solid elements to describe the passive behavior of the muscle. The active behavior of the muscle was applied to the 1D elements. The three-element Hill muscle model [27] was employed to describe the active mechanical response of the muscle. Hill's model consists of a Contractile Element (CE), a non-linear spring in series (SE) and a non-linear spring in parallel (PE) as illustrated in Figure 2.

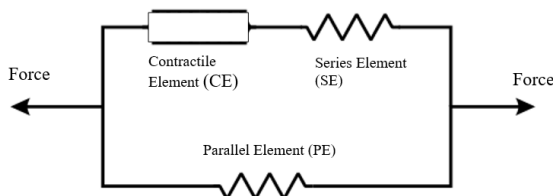


Figure 2: Hill's muscle model.

The contractile element (CE) is responsible for the active tension of the muscle. It generates force within the activated muscle [28]. Force generation within the CE is a function of activation kinetics (a), force-length properties (F^L), and force-velocity properties (F^v). The total active force generated in the CE can be expressed as a product of these components, as shown in Equation (1) [17]:

$$F^{CE}(L, v) = a(t) \sigma_0 F^L(L) F^v(v) \quad (1)$$

Experimental studies [17] have demonstrated that the active force depends on the muscle's length, reaching its maximum at the optimal muscle length L_{opt} . The relationship between the force and muscle length, known as the force-length relationship, is described in Equation (2):

$$F^L(L) = e^{-\left(\frac{\left(\frac{L}{L_{opt}} - 1\right)}{csh}\right)^2} \quad (2)$$

where L is the total muscle's length and csh is a shape factor.

In addition to the muscle length, the active force generated by the CE also depends on the shortening or lengthening velocity of the muscle fibers. This dependency is captured by the force-velocity relationship, which is given in Equations (3)–(5). As shown in these equations, the force decreases with increasing shortening velocity, whereas it increases asymptotically with lengthening velocity [17]:

$$F^v(v) = 0 \quad v \leq -l \quad (3)$$

$$F^v(v) = \frac{I + v}{I - \frac{v}{C_{short}}} \quad -lv < v \leq 0, \quad v = \frac{V}{V_0} \quad (4)$$

$$F^v(v) = x = \frac{I + v \frac{C_{mv} l}{C_{length}}}{I + \frac{v}{C_{length}}} \quad v > 0 \quad (5)$$

where V_0 is the maximum shortening velocity of the muscle.

The SE smoothens rapid changes in muscle tension and provides an energy-storing mechanism, representing the tendon elasticity observed in real muscles. This reflects physiological tendon behavior rather than a numerical artifact [28]. The PE component is responsible for passive tension, which is the resistance a muscle generates when stretched without activation, mainly due to the elasticity of its connective

tissues. The total muscle force in a muscle can be expressed as the sum of the forces in the CE and the PE.

2.2 Model setup for a simple impact test of an active muscle

The developed active muscle model was validated with the results published by Iwamoto *et al.*, [10]. The stiffness characteristics were also studied from this simple validation test. The model set up for the validation is shown in Figure 3. The simple biceps brachii muscle model was placed on top of a rigid wall. Both ends of the model were fixed in all directions to mimic isometric contraction. An indentation force, ranging from 0–25 Newtons, was applied to the middle of the muscle.

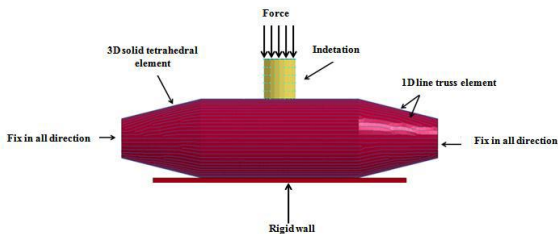


Figure 3: Model set up for stiffness validation of active muscle.

2.3 Model setup to simulate concentric and eccentric contraction

To determine whether the developed active muscle model could mimic the concentric (shortening) and eccentric (lengthening) contraction behavior of muscles, another set of simulations was conducted. For these simulations, the simple muscle model was fixed in all directions at its right end, as shown in Figure 4. Within the LS-Dyna material keyword, the contraction velocity was assigned a positive value to represent concentric simulations and a negative value for eccentric contractions. Specifically, a normalized value of +1.0 was used for concentric shortening, while a value of -1.0 was used for eccentric lengthening, which aligns with previous experimental findings [16].



Figure 4: Concentric and eccentric contraction simulation setup.

2.4 Inclusion of muscle models in THUMS

The validated muscle model from the previous section was employed. Twenty-four muscle models, representing the major lower extremity muscle groups critical for pedestrian biomechanics during impact, were inserted into both legs of THUMS as shown in Figure 5. This selection included muscles in the thigh, knee, pelvis, and shank, ensuring a realistic representation while keeping computational costs manageable. The muscles were attached to the bone by extending the fibers and creating shared nodes between the muscle and the bone, which is also depicted in Figure 5.

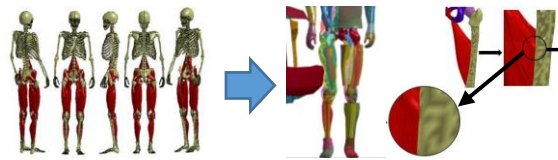


Figure 5: THUMS model with active skeletal muscle in lower extremities.

2.5 Crash simulation set up

The pedestrian-vehicle crash simulation was set up as illustrated in Figure 6. The pickup truck model, which was validated against the US NCAP crash test, was obtained from the National Crash Analysis Center [29]. The THUMS had also been validated as reported in [13]. In the simulation, THUMS with active muscle models was positioned at the centerline of the pickup truck. The contact friction coefficient between the vehicle and THUMS was set to 0.3 [30], while the ground friction coefficient was 0.9. An impact speed of 20 km/h was selected for the primary simulation, as studies have shown that the average vehicle speed in cities is between 17.6–21.8 km/h [3], [31]. Muscle activation levels were determined based on studies of muscle activities in daily life [32]. While research by Tikkanen *et al.*, reported that standing and walking typically involve 5–21% muscle activation, panic situations can lead to higher levels. Consequently, this study used four levels of muscle activation: 5%, 20%, 50%, and 100%. A secondary simulation was also conducted at an impact speed of 30 km/h, which is the typical speed limit in community areas. In total, seven simulation cases were analyzed.

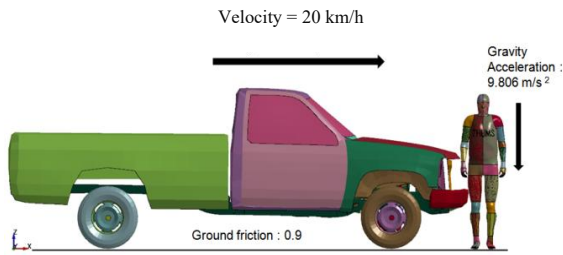


Figure 6: Pedestrian-vehicle simulation set up.

2.6 Injury measures

The THUMS model was prepared to measure pedestrian injury metrics, including head acceleration, lower extremity bending, and force. Head acceleration was measured at the head's center of gravity (C.G.) to minimize the effect of head rotation. This measurement was used to calculate the Head Injury Criterion (HIC) for the pedestrian [30]. Figure 7 shows the location of the head's C.G. in the THUMS model. To measure bending and force, the lower extremities were sectioned as shown in Figure 7. A cross-section was defined by a set of shell and solid elements connected by their respective nodes. A total of 32 cross-sections were defined and distributed along the femur, tibia, and knee to capture local bending and shear at injury-prone regions, consistent with Euro NCAP injury protocols. Tibia acceleration was measured by accelerometers attached at point P9, as indicated in Figure 7. Knee shearing displacement was obtained by measuring the change in distance "D" between the lines joining points P1-P2 and P3-P4, also specified in Figure 7. Finally, the knee bending angle was measured as the angle between the vectors from P5 to P6 and P7 to P8 [33].

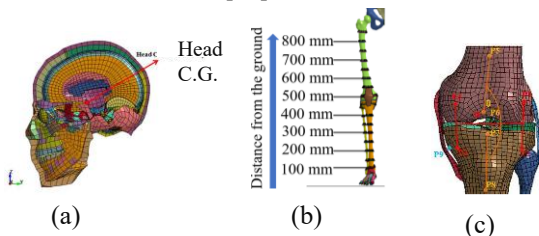


Figure 7: Preparation for injury measures for (a) head acceleration, (b) lower extremities bending (c) knee shear displacement and angle.

3 Results

3.1 Active muscle model validation

The current study's simulation results captured the stiffness change with a $\pm 15\%$ margin, showing reasonably good agreement with the findings of Iwamoto *et al.* [10], as depicted in Figure 8. This level of agreement is considered acceptable within the field of computational biomechanics, where model validation often accounts for inherent complexities and measurement variability in biological systems. Figure 9 shows the stiffness variation of a simple muscle model in isometric contraction based on different activation levels. The stiffness value was calculated when the muscle reached its maximum displacement. It was found that the muscle's stiffness increased as the activation level also increased.

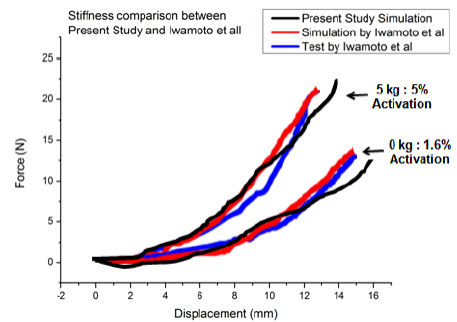


Figure 8: Stiffness comparison between the present study and Iwamoto *et al.* [10].

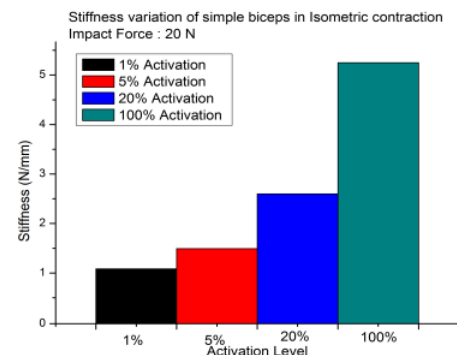


Figure 9: Stiffness variation for different levels of activation.

3.2 Concentric and eccentric contraction simulation

Concentric and eccentric contraction characteristics were simulated. The model can capture the contraction behavior of the muscles as shown in Figure 10.

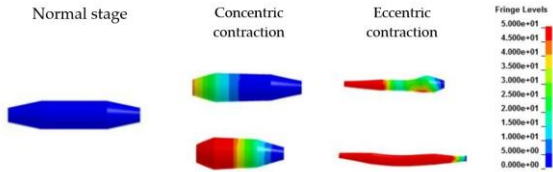


Figure 10: Total displacement of the simple biceps brachii muscle in concentric and eccentric contractions at 10% activation.

3.3 Vehicle-Pedestrian crash simulation results

3.3.1 Overall pedestrian kinematic behavior

Figure 11 illustrates a comparison of pedestrian kinematics obtained from THUMS with varying muscle activation levels. Overall, the kinematics were similar across scenarios and consistent with the findings of Han *et al.* [30], [31]. Initially, the vehicle's bumper struck the right leg of THUMS, which caused the right thigh to bend. The upper extremity and pelvis were then impacted by the bonnet leading edge. Subsequently, the upper body began to bend around the front of the vehicle, lifting THUMS's right foot off the ground, with both legs eventually leaving the ground. The torso then impacted the bonnet, followed by the head striking the bonnet. The timing and location of the head impact varied slightly depending on the muscle activation level. Specifically, the model without muscle activation impacted the bonnet slightly later (at 172 ms) compared to the model with 100% muscle activation (at 168 ms).

Figure 12 depicts the head trajectory obtained from various activation levels. Differences become noticeable as the head moves downward toward the bonnet. The THUMS with active muscles had a head impact location slightly closer to the bonnet leading edge. Higher activation levels also slightly reduced the time to head impact. Differences in kinematics are also observed in the lower extremities, as shown in Figure 13, which illustrates the trajectory of the length between the right and left toes. Front-end impact caused the right foot to roll inward toward the left, reducing toe length in the x-direction while z-length

remained near zero as both toes stayed on the ground. As the feet lifted, the right foot moved beneath the left, and z-length increased until both were airborne, then decreased. For the full muscle activation case, maximum overlap occurred at $x \approx -85.2$ mm and $z \approx 200$ mm, with a pronation angle of 24° , below the allowable limit of 30° . Overall kinematics were similar across activation levels, but differences in x- and z-lengths became more pronounced at higher activation levels, especially after both feet left the ground.

















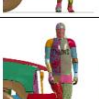



Time Activation level	20 ms	60 ms	120 ms	180 ms
No active muscle				
5% muscle activation				
20% muscle activation				
50% muscle activation				
100 % muscle activation				

Figure 11: Comparison of pedestrian kinematics for different levels of muscle activation.

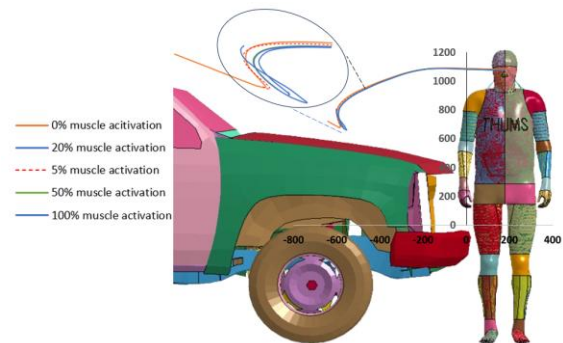


Figure 11: Comparison of pedestrian kinematics for different levels of muscle activation.

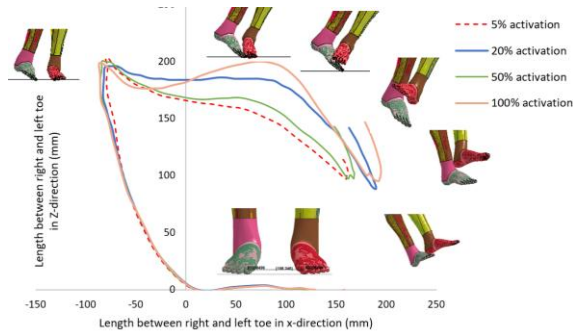


Figure 13: Comparison of change in length between right and left toes during collision.

3.3.2 Contact force between pedestrian lower extremities and pick-up truck

The resultant contact reaction force during the simulation is depicted in Figure 14. The trends of the contact reaction force between the model without muscle activation and the model with muscle activation were quite similar. Initially, the contact force increased rapidly, reaching its first peak caused by the bumper colliding with the thigh. As the lower extremity on the impact side began to bend and gain speed, the contact force gradually decreased. Subsequently, the contact force rose again, reaching a second peak when the upper body contacted the vehicle's bonnet. Small peaks of force occurred thereafter due to contact between the right and left legs, followed by a gradual decrease in contact force. The first peak contact force of the model with active muscle activation (6.7 kN) was higher than that of the model without activation (4.9 kN). This occurs because muscle contraction increases limb stiffness, reducing deformation and transferring greater reaction force at the point of contact. The observed increase in contact force with activation is consistent with Soni *et al.* [11], who reported stiffer knee responses under muscle contraction. Minor differences were observed among the different levels of muscle activation. When considering the impact speed of 30 km/h, slight variations in resultant force were observed, with the model at 100% muscle activation showing slightly higher contact force (11 kN). Overall, higher impact speeds also led to higher contact forces.

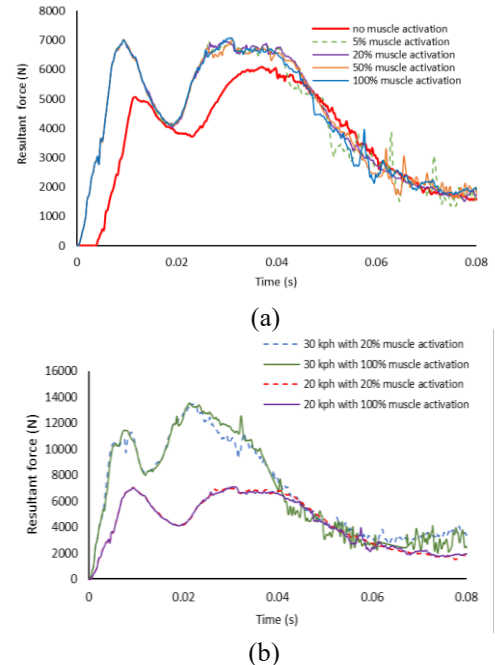
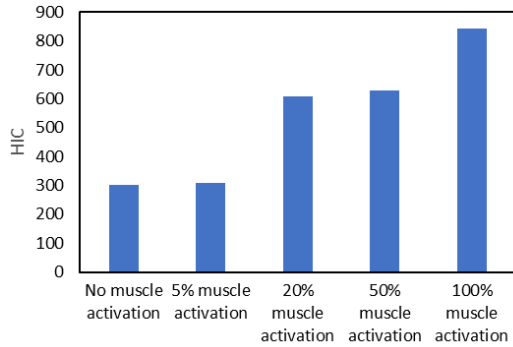


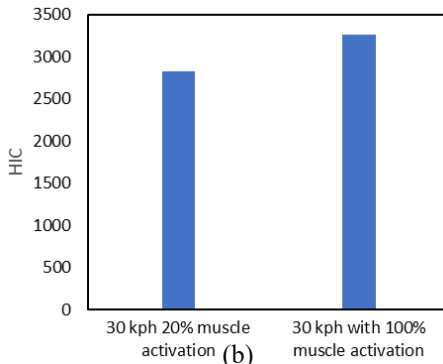
Figure 14: Comparison of the resultant contact force: (a) between models with and without muscle activation at 20 km/h; (b) among different muscle activation levels at 20 and 30 km/h impact speeds.

3.3.3 Head injury criteria

Head Injury Criteria (HIC) were calculated and are depicted in Figure 15. Figure 15(a) shows a comparison of the HIC values calculated from the model with a 20 km/h impact speed. The model without muscle activation exhibited the lowest HIC value (300.9), which is consistent with the findings of Han *et al.*, at an impact speed of 20 km/h [31]. The fully activated model showed the highest HIC value (841.4). HIC values increased with the level of muscle activation. This increase is attributed to the higher stiffness of muscles, which results in a higher head impact velocity and consequently a higher head acceleration. Similarly, as shown in Figure 15(b), the trend in HIC values remained consistent at an impact speed of 30 km/h. However, the HIC value for full muscle activation (3261) was significantly higher, mainly due to the increased impact speed [31].



(a)



(b)

Figure 15: Comparison of the Head injury criteria (HIC): (a) between models with and without muscle activation at 20 km/h; (b) among different muscle activation levels at 30 km/h impact speeds.

3.3.4 Lower extremity injury measures

The lower extremities were divided into the femur, knee, and tibia. Bending moments were obtained for the femur and tibia, while the shearing distance and bending angle were obtained for the knee. Figure 16 provides a comparison of the maximum resultant moments in the femur and tibia. It is evident that the overall resultant moment along the right femur of the model without muscles was significantly lower (293 kN/mm) than in the model with muscles (373.5 kN/mm). However, muscle activation levels did not substantially affect the bending moment.

At a higher impact speed (30 km/h), differences in the bending moment became noticeable at the tibia for different activation levels. Higher activation levels resulted in slightly lower bending moments at the tibia during the 30 km/h impact.

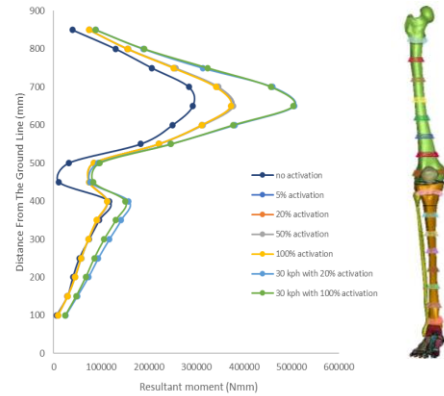
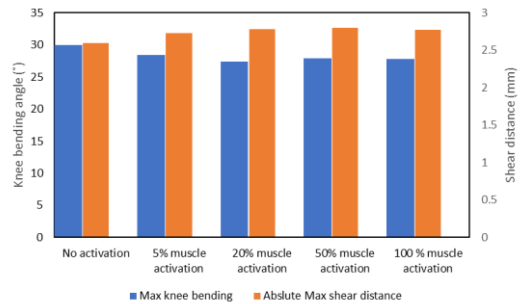
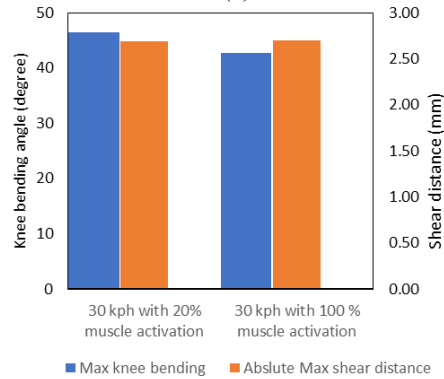


Figure 16: Comparison of maximum resultant moment for different levels of muscle activation.



(a)



(b)

Figure 17: Comparison of maximum knee bending angle, maximum shear distance for different levels of muscle activation (a) with impact speed of 20 km/h (b) with impact speed of 30 km/h.

Figure 17 presents a comparison of the maximum knee shearing distance and bending angle. The model without active muscles exhibited a lower shearing distance (2.6 mm, considering magnitude only) compared to the model with fully activated active muscles (2.8 mm). Models with higher

activation levels showed slightly higher maximum shearing distances. Importantly, all knee shearing distances in this simulation remained within the Euro NCAP standard for knee injury, which sets a limit of 3.5 mm, with an upper limit of 6 mm [34].

The maximum bending angle was highest for the model without active muscles (30°) compared to that with active muscle activation (27.8°). This maximum bending angle slightly decreased with increasing levels of activation. Similar trends were observed at the impact speed of 30 km/h. However, all results for the maximum knee bending angle exceeded the Euro NCAP limit of 15 degrees [34].

4 Discussion

The pickup truck collision with the pedestrian human body model, both with and without muscle activation, exhibited similar kinematics at the beginning of the impact when the muscle was just activated. Some differences were observed after the impact when the lower extremities started to bend around the front of the vehicle. The head and foot trajectories differed after both legs left the ground. The difference in head trajectory also led to different head impact times. The model with muscle activation made head contact with the bonnet earlier, resulting in higher head acceleration and, consequently, a higher HIC. The maximum bending moment was obtained from various locations of the lower extremities. It was found that the model without active muscle exhibited a lower bending moment. The difference was clearly observed around the area where the bumper impacted the right femur and tibia. These results were mainly caused by the contraction of the muscles in the femur. When the muscles contracted, the femur experienced torque from the muscles because the contraction force among these muscles varied based on their architectural properties. This is why the model without muscles experienced a lower resultant moment than the model with muscles. The active muscle contraction made the knee joint stiffer than the knee joint without muscle activation. The model with active muscle showed a lower maximum knee bending angle but a slightly higher shear distance. Due to muscle contraction, the knee of THUMS with active muscle was more difficult to bend compared to the THUMS without active muscle. Consequently, the impact force from the vehicle was more transferred as shear force in the knee rather than producing bending deformation. All results of the maximum knee bending angle exceeded the Euro NCAP limit of 15 degrees [34].

When comparing the effect of different levels of muscle activation on kinematics and injury measures, it was found that the muscle activation level slightly affected the head and foot trajectories during impact. Higher levels of activation led to higher levels of HIC values. The knee bending angle and shear distance were also slightly affected by the level of muscle activation; increasing the level of activation resulted in decreased knee bending but increased shear distance. However, the level of muscle activation had little effect on contact force and bending moment. At higher impact speeds (i.e., 30 km/h), the effect of the level of activation on kinematics and injury response was similar to that at 20 km/h.

Live pedestrian crash tests on human subjects are not ethically feasible; therefore, this study relied on a validated human body model. Although direct human data are not available, the trends observed are consistent with experimental findings and biomechanical studies [8]–[11], supporting the reliability of this simulation-based approach. A limitation of the present muscle activation model is that it assumes uniform activation across all muscles. In reality, activation is non-uniform, with different muscle groups recruited at varying intensities and timings depending on reflexes and posture. EMG studies of panic reflexes, for example, show preferential activation of extensors, which may redistribute joint loading. As a result, our model may over- or underestimate local joint stresses, although the overall trends remain valid.

5 Conclusions

This study addresses a key limitation in pedestrian human body models by integrating active muscle representation to examine its role in low-speed collisions. A skeletal muscle model combining 3D solid and 1D line elements was developed and validated using Ogden and Hill-type formulations. Results from four activation levels (5%, 20%, 50%, 100%) show that active muscles significantly alter pedestrian kinematics and injury outcomes. At 20 km/h, the fully active model produced a ~179% increase in HIC, a 7.7% increase in knee shear distance, and a 10% decrease in knee bending angle compared with the passive model. Similar trends were observed at 30 km/h. These findings demonstrate that active muscle models provide a more biofidelic representation of human response in low-speed collisions, supporting the development of safety features such as deployable bonnets and pre-crash restraint systems. Overall, the results highlight the importance of including active muscle representation



in pedestrian models for more accurate injury prediction.

Author Contributions

J.C., B.M.: Conceptualization; J.C., B.M., I.P.P.: methodology; I.P.P. and J.C. software; I.P.P.: validation; I.P.P. and J.C.: formal analysis; I.P.P.: investigation; B.M., J.C.: resources; I.P.P. and J.C. writing—original draft preparation; J.C.: writing—review and editing; J.C.: visualization; B.M., J.C.: supervision. All authors have read and agreed to the published version of the manuscript.

Conflicts of Interest

The authors declare no conflict of interest.

Declaration of generative AI and AI-assisted technologies in the writing process

The authors utilized the ChatGPT tool to enhance the language and readability of the manuscript

References

- [1] World Health Organization, *Global Status Report on Road Safety 2018*. Geneva, Switzerland: World Health Organization, 2018.
- [2] Department of Land Transport. "Transport Statistics Report 2020." Bangkok, Thailand, 2021. [Online]. Available: www.dlt.go.th/statistics/
- [3] Office of Transport and Traffic Policy and Planning. "Summary of the Survey Results on the Average Speed of Private Cars in Bangkok in 2020." Bangkok, Thailand, 2021. [Online]. Available: <https://www.otp.go.th/post/view/4505>
- [4] T. Maeno and J. Hasegawa, "Development of a finite element model of the total human model for safety (THUMS) and application to car-pedestrian impacts," presented at the 17th International Technical Conference on the Enhanced Safety of Vehicles, Amsterdam, Netherlands, Jun. 4–7, 2001.
- [5] S. Robin, "HUMOS: Human model for safety — A joint effort towards the development of refined human-like car occupant models," presented at the 17th International Technical Conference on the Enhanced Safety of Vehicles, Amsterdam, Netherlands, Jun. 4–7, 2001.
- [6] J. Combet, "Current status and future plans of the GHBMC (Global Human Body Models Consortium)," presented at the 7th International Symposium on Human Modelling and Simulation in Automotive Engineering, Oct. 18–19, 2018.
- [7] W. C. Bowman, A. A. J. Goldberg, and C. Raper, "A comparison between the effects of a tetanus and the effects of sympathomimetic amines on fast and slow contracting mammalian muscles," *British Journal of Pharmacology*, vol. 19, pp. 464–484, 1962.
- [8] V. S. Alvarez, M. Fahlstedt, P. Halldin, and S. Kleiven, "Importance of neck muscle tonus in head kinematics during pedestrian accidents," presented at the International Research Council on Biomechanics of Injury, Gothenburg, Sweden, Sept. 11–13, 2013.
- [9] S. Hedenstierna, P. Halldin, and K. Brolin, "Development and evaluation of a continuum neck muscle model," presented at the 6th European LS-DYNA Users Conference, Gothenburg, Sweden, 2007.
- [10] M. Iwamoto and Y. Nakahira, "A preliminary study to investigate muscular effects for pedestrian kinematics and injuries using active THUMS," presented at the International Research Council on Biomechanics of Injury, Berlin, Germany, Sept. 10–12, 2014.
- [11] A. Soni, A. Chawla, S. Mukherjee, and R. Malhotra, "Response of lower extremity in car-pedestrian impact – Influence of muscle contraction," presented at the International Research Council on Biomechanics of Injury, Bern, Switzerland, Sept. 17–19, 2008.
- [12] I. P. A. Putra et al., "Finite element human body models with active reflexive muscles suitable for sex-based whiplash injury prediction," *Frontiers in Bioengineering and Biotechnology*, vol. 10, 2022, doi: 10.3389/fbioe.2022.968939.
- [13] Toyota Motor Corporation, *THUMS Documentation – AM50 Pedestrian/Occupant Model Academic Version 4.0*, Oct. 2011.
- [14] N. Mitsuhashi et al., "BodyParts3D: 3D structure database for anatomical concepts," *Nucleic Acids Research*, vol. 37, pp. D782–D785, 2009.
- [15] T. Nagaoka et al., "Development of realistic high-resolution whole-body voxel models of Japanese adult males and females of average height and weight, and application of models to radio-frequency electromagnetic-field dosimetry," *Physics in Medicine & Biology*, vol. 49, pp. 1–15, 2004.

- [16] C. Gans, "Fiber architecture and muscle function," *Exercise and Sport Sciences Reviews*, vol. 10, pp. 160–207, 1982.
- [17] S. C. Bodine et al., "Architectural, histochemical, and contractile characteristics of a unique biarticular muscle: The cat semitendinosus," *Journal of Neurophysiology*, vol. 48, pp. 192–201, 1982.
- [18] R. J. Maughan, J. Watson, and J. Weir, "Strength and cross-sectional area of human skeletal muscle," *Journal of Physiology*, vol. 338, pp. 37–49, 1983.
- [19] D. Lee et al., "A three-dimensional approach to pennation angle estimation for human skeletal muscle," *Computer Methods in Biomechanics and Biomedical Engineering*, pp. 1–11, 2014.
- [20] S. R. Ward et al., "Are current measurements of lower extremity muscle architecture accurate?," *Clinical Orthopaedics and Related Research*, vol. 467, pp. 1074–1082, 2009.
- [21] E. M. Arnold et al., "A model of the lower limb for analysis of human movement," *Annals of Biomedical Engineering*, vol. 38, pp. 269–279, 2010, doi: 10.1007/s10439-009-9852-5.
- [22] R. L. Lieber, *Skeletal Muscle Structure, Function, and Plasticity: The Physiological Basis of Rehabilitation*. Baltimore, MD: Lippincott Williams & Wilkins, 2002.
- [23] R. A. Brand et al., "A model of lower extremity muscular anatomy," *Journal of Biomechanical Engineering*, vol. 104, pp. 304–310, 1982.
- [24] S. L. Delp et al., "An interactive graphics-based model of the lower extremity to study orthopaedic surgical procedures," *IEEE Transactions on Biomedical Engineering*, vol. 37, pp. 757–767, 1990.
- [25] J. A. Friederich and R. A. Brand, "Muscle fiber architecture in the human lower limb," *Journal of Biomechanics*, vol. 23, pp. 91–95, 1990.
- [26] M. D. K. Horsman, "The twente lower extremity model: Consistent dynamic simulation of the human locomotor apparatus," Ph.D. dissertation, University of Twente, Enschede, Netherlands, 2007.
- [27] A. V. Hill, "The heat of shortening and the dynamic constants of muscle," *Proceedings of the Royal Society of London. Series B, Biological Sciences*, vol. 126, no. 843, pp. 136–195, 1938.
- [28] Y. Yongtaou, "Soft tissue modelling and facial movement simulation using finite element method," Ph.D. dissertation, Cardiff University, Cardiff, U.K., 2010.
- [29] National Crash Analysis Center, "Finite Element Model of C1500 Pickup Truck, Model Year 1994, Version 7," Washington, DC: The George Washington University, Federal Highway Administration and National Highway Traffic Safety Administration, U.S. Department of Transportation, 2008.
- [30] Y. Han et al., "Finite element analysis of kinematic behaviour and injuries to pedestrians in vehicle collisions," *International Journal of Crashworthiness*, vol. 17, pp. 141–152, 2011.
- [31] Y. Han et al., "Effects of vehicle impact velocity and vehicle front-end shapes on pedestrian injury risk," *Traffic Injury Prevention*, vol. 13, pp. 507–518, 2012.
- [32] O. Tikkanen et al., "Muscle activity and inactivity periods during normal daily life," *PLoS ONE*, vol. 8, no. 1, 2013, doi: 10.1371/journal.pone.0052228.
- [33] L. Martínez et al., "Influence of vehicle shape and stiffness on the pedestrian lower extremity injuries: Review of current pedestrian lower leg test procedure," presented at the International Research Council on Biomechanics of Injury, Berlin, Germany, Sep. 10–12, 2008.
- [34] European New Car Assessment Programme (Euro NCAP), "Assessment Protocol – Vulnerable Road User Protection, Version 11.4," 2023.